JGR Atmospheres

RESEARCH ARTICLE
10.1029/2022JD037280

Key Points:

- Intensifying storms have a lower degree of asymmetry of the surface inflow angle than steady-state storms under moderate wind shear
- The degree of downshear versus upshear asymmetry of the surface inflow angle increases with the shear magnitude
- The degree of shear-relative asymmetry of the surface inflow angle is larger in the outer core region than in the eyewall region

Correspondence to:
J. A. Zhang,
jun.zhang@noaa.gov

Citation:
Ming, J., Liu, R., Zhang, J. A., & Rogers, R. F. (2022). The shear-relative variation of inflow angle and its relationship to tropical cyclone intensification. *Journal of Geophysical Research: Atmospheres*, *127*, e2022JD037280s. https://doi.org/10.1029/2022JD037280

Received 10 JUN 2022
Accepted 2 AUG 2022

The Shear-Relative Variation of Inflow Angle and Its Relationship to Tropical Cyclone Intensification

Jie Ming[1,2], Ruixue Liu[1,2], Jun A. Zhang[3,4], and Robert F. Rogers[3]

[1]Key Laboratory of Mesoscale Severe Weather/MOE and School of Atmospheric Science, Nanjing University, Nanjing, China, [2]State Key Laboratory of Severe Weather and Joint Center for Atmospheric Radar Research of CMA/NJU, Beijing, China, [3]NOAA/Atlantic Oceanographic and Meteorological Laboratory/Hurricane Research Division, Miami, FL, USA, [4]University of Miami/Cooperative Institute for Marine and Atmospheric Studies, Miami, FL, USA

Abstract Characterizing inflow structure is important to better represent tropical cyclone impacts in numerical models. While much research has considered the impact of storm translation on the distribution of inflow angle, comparatively less research has examined its distribution relative to the environmental wind shear. This study analyzes data from 3,655 dropsondes in 44 storms to investigate the radial and shear-relative distribution of surface inflow angle. Emphasis is placed on its relationship with intensity change. The results show that the radial variation in the inflow angle is small and not significantly dependent on the shear magnitude or intensity change rate. In contrast, the azimuthal distribution of the inflow angle shows a significant asymmetry, with the amplitude of the asymmetry increasing with shear magnitude. The maximum inflow angle is located in the downshear side. The degree of asymmetry is larger in the outer core than in the eyewall. Intensifying storms have a smaller degree of asymmetry than steady-state storms under moderate shear.

Plain Language Summary The inflow angle represents the degree that the wind vector deviates from the tangential wind. It is an important factor for the successful modeling of tropical cyclone evolution and storm surge. Although the inflow angle in the storm-relative framework and its variation with storm intensity have been documented in the past, it is still unknown how the inflow angle varies with intensity change in different variations of environmental wind speed and direction with height. This study uses the observational data from aircraft to investigate the characteristics of the radial and azimuthal distributions of inflow angle in storms with different values of environmental wind variation and intensity change rates. The results show minor differences in inflow angle with increasing radius from the storm center, but more significant differences in inflow angle moving around the storm. The degree of asymmetry increases with the magnitude of environmental wind variation and decreases with the storm intensity change rate. The inflow angle is more asymmetric in the outer core region than in the eyewall region.

1. Introduction

Wave and storm surge models are key tools for predicting the impacts of landfalling tropical cyclones (TCs). These models are usually forced by the surface wind field from either a full physics atmospheric model or parametric wind model. Accurate representation of the surface wind vector in these models is important for improving wave and surge forecasts in TC conditions. Several parametric wind speed models for TCs, in particular axisymmetric models, have been developed in the past based on theory and observations (Chavas & Lin, 2016; Holland, 1980; Willoughby, 1990). However, two-dimensional parametric surface wind models that predict both the wind speed and direction have been limited mainly due to limited observations of surface wind direction in TCs (Zhang & Uhlhorn, 2012, hereafter Z12). The inflow angle, defined as the arctangent of the ratio of radial to tangential wind components, has been known to be crucial for storm surge and wave modeling (Fan et al., 2009; Houston et al., 1999). Peng et al. (2006) found that larger inflow angles can induce larger sea level surge in storm surge models. Zhao and Hong (2011) indicated that increasing inflow angle results in increasing maximum significant wave height and larger quadrant differences of mean significant wave height. Inflow angle is thus an important dynamic parameter for the development and evaluation of both storm-surge and TC forecast models (Aijaz et al., 2019; Bryan, 2012; Fan et al., 2020; Kepert, 2010; Wang et al., 2018; Zhang et al., 2015, 2017).

Table 1
Storm Information and Numbers of Flights and Dropsondes

Storm name	Year	Storm intensity (kt)	Number of flights	Number of sondes
Dennis	999	65–90	12	124
Floyd	999	90–135	10	63
Lili	2002	34–124	17	94
Fabian	2003	105–120	9	49
Isabel	2003	131–140	11	55
Frances	2004	43–64	18	175
Ivan	2004	90–145	30	232
Jeanne	2004	34–100	15	70
Dennis	2005	67–125	15	64
Katrina	2005	45–150	17	72
Rita	2005	49–154	23	234
Wilma	2005	145–153	1	2
Dean	2007	80–150	8	25
Felix	2007	145–150	3	12
Gustav	2008	41–122	15	99
Earl	2010	50–121	26	200
Irene	2011	45–105	24	355
Isaac	2012	45–70	15	319
Leslie	2012	55–60	4	29
Sandy	2012	60–81	9	115
Ingrid	2013	38–74	8	93
Arthur	2014	41–83	9	100
Bertha	2014	47–70	5	71
Cristobal	2014	34–70	9	117
Edouard	2014	72–102	8	79
Gonzalo	2014	107–125	3	12
Danny	2015	34–106	7	65
Joaquin	2015	82–134	5	36
Earl	2016	50–70	3	19
Matthew	2016	67–133	15	80
Harvey	2017	34–110	8	29
Irma	2017	98–155	15	49
Jose	2017	70–80	2	7
Maria	2017	65–150	4	27
Nate	2017	35–80	6	42
Chris	2018	35–60	3	13
Florence	2018	57–124	12	95
Gordon	2018	50–57	3	9
Isaac	2018	38–55	3	19
Michael	2018	82–126	7	69
Barry	2019	34–52	8	87
Dorian	2019	45–116	12	71

In the Sea, Lake and Overland Surge from Hurricanes (SLOSH) model, the inflow angle is parameterized as a function of radial distance without consideration of the azimuthal variation of the inflow angle (Bretschneider, 1972; Lin & Chavas, 2012; Queensland Government, 2001; Zhang et al., 2016). Values of the inflow angle in SLOSH were set based on a limited number of numerical and observational studies (Malkus & Riehl, 1960; Powell, 1982; Powell et al., 2009). Z12 documented the storm-motion-relative distribution of the surface inflow angle using ∼1,800 dropsondes collected in TCs and pointed out that the degree of azimuthal asymmetry in inflow angle increases with the storm motion speed. Another significant contributor to asymmetries in storm structure is environmental wind shear. The relationship between wind shear and inflow angle has yet to be examined, however. Furthermore, environmental wind shear is a very important factor influencing the structure of a TC. How the inflow angle distribution varies in storms under different environmental wind shear conditions remains to be explored.

It is well known that environmental wind shear imposes a wavenumber-1 asymmetry on TC structure. Previous studies have found that the downshear side of a storm tends to have stronger upward motion (Black et al., 2002; DeHart et al., 2014; Reasor et al., 2009), higher convective available potential energy (CAPE) and larger helicity (Molinari & Vollaro, 2008; Molinari et al., 2012), and a deeper boundary layer (Zhang et al., 2013) than the upshear side. Severe and deep convection depicted by lightning and heavy rainfall also tends to occur downshear, with the maximum rainfall being in the downshear-left quadrant (Corbosiero & Molinari, 2002; Reasor et al., 2013; Rogers et al., 2016). Analyses of Doppler radar and dropsonde data indicate that convection is initiated in the downshear-right quadrant and becomes mature in the downshear-left quadrant, where the boundary layer convergence is also significant (DeHart et al., 2014; Reasor et al., 2013; Wadler et al., 2018; Zhang et al., 2013). While one could infer the relationship between inflow angle and vertical shear direction based on this previous work, no studies have quantified the relationship between vertical shear and inflow angle.

TCs under large environmental shear typically weaken, while TCs under weak shear tend to intensify rapidly given otherwise favorable environmental conditions of sea-surface temperature and low- and mid-level humidity (Frank & Ritchie, 2001; Onderlinde & Nolan, 2017; Tao & Zhang, 2014). Previous studies have shown that the intensity change of a TC under moderate shear, typically defined as 850–200 hPa shear magnitude between 5 and 10 m s^{-1} (Molinari et al., 2004; Rios-Berrios et al., 2018), is comparatively uncertain due to vortex and shear interactions and various distributions of convection (e.g., Rios-Berrios et al., 2018; Rogers et al., 2016, 2020; Ryglicki et al., 2018, 2019). Boundary layer processes such as vertical turbulent mixing and enthalpy transfer also modulate the TC intensity change in shear by affecting the inflow strength, convective initiation, and recovery of downdraft-induced low entropy air (Nguyen et al., 2019; Wadler et al., 2021; Zhang & Rogers, 2019). For instance, the magnitude of inflow is related to the length of time air parcels travel from the outer core to the eyewall region of a hurricane, which is important for the recovery process. It is thus important to understand the shear-relative distribution of boundary layer inflow and its relationship to TC intensity change.

The objectives of the present study are as follows:

Table 1
Continued

Storm name	Year	Storm intensity (kt)	Number of flights	Number of sondes
Jerry	2019	50–90	6	37
Lorenzo	2019	90–117	5	41
Totals			448	3,655

1. To document the inflow angle distribution relative to the environmental wind shear.
2. To investigate the variation in the magnitude of axisymmetric inflow angle and the degree of shear-relative asymmetry as a function of shear magnitude.
3. To investigate the possible linkage between the radial and azimuthal distribution of inflow angle and TC intensity change.

2. Data and Methodology

GPS dropsonde data are analyzed to study the characteristics of the surface inflow angle. The dropsonde data were obtained in 44 TCs from 1999 to 2019 during research and reconnaissance missions over the Atlantic basin including dropsondes deployed by WP-3D, G-IV, Global Hawk, DC-8, and Airforce flights. A GPS dropsonde measures vertical profiles of wind velocities, air temperature, relative humidity, and pressure with a sampling rate of 2 Hz. Information on the detailed dropsonde instrumentation and accuracy is found in Hock and Franklin (1999). The dropsonde data was post-processed and quality-controlled using the National Center for Atmospheric Research (NCAR)'s Atmospheric Sounding Processing Environment (ASPEN) software (Barnes, 2008; Zhang et al., 2013, 2020). Table 1 summarizes the storm name, year, intensity range, number of flights, and number of dropsondes. To study the surface inflow angle distribution, only dropsondes that have measurements near the surface (10 m altitude) were used in this study. The horizontal wind components are linearly interpolated to the 10-m altitude to derive the surface inflow angle. The total number of quality-controlled dropsondes that meet these criteria is 3,655.

The frequency distributions of the surface inflow angle and storm characteristics, including the environmental vertical wind shear magnitude, storm intensity (V_{max}), radius of maximum surface wind speed (R_{max}), and 12 hr intensity change which is the difference in V_{max} between the dropsonde time and 12 hr after, are presented in Figure 1. The environmental vertical wind shear data is obtained from the Statistical Hurricane Intensity Prediction Scheme (SHIPS, DeMaria et al., 2005). The magnitude and direction of the vertical shear of horizontal wind between 850 and 200 hPa are calculated by subtracting the averaged wind vector in a 200–800 km annulus from the storm center at 200 hPa from that at 850 hPa. The V_{max} values are obtained from the best-track database interpolated to the time of dropsonde observations and 12 hr after that time. R_{max} is determined from near-concurrent surface winds measured by the Stepped Frequency Microwave Radiometer. This study focuses on TCs of tropical storm strength or greater (i.e., $V_{max} > 34$ kt) with shear magnitudes ranging between 0 and 16 m s^{-1}. The data were averaged as a function of radius (r) normalized by R_{max} (i.e., $r^* = r/R_{max}$) with a radial bin width of $r^* = 0.2$ to exclude the effect of storm size and illustrate the radial variation of the axisymmetric inflow angle. The asymmetric distribution of inflow angle is examined in a shear-relative framework for groups with different shear magnitudes and radii. The shear-relative data distribution is shown in Figure 2.

3. Results

3.1. Axisymmetric Distribution

Figure 3 shows the axisymmetric inflow angle as a function of radius, magnitude of vertical shear, and TC intensity change. The mean value of the inflow angle is −21.12° from all samples including all radii and azimuths (Figure 3a), which is in agreement with previous studies (e.g., Z12, Powell et al., 2009). (The negative value of inflow angle is defined as the inflow, and the larger value means stronger inflow.) This result indicates that the mean radial flow of all samples is inflow. Figure 3b shows the azimuthally-averaged inflow angle as a function of r^*. The inflow angle magnitude shows an increasing trend with increasing r^* (Figure 3b), which also agrees well with the axisymmetric characteristic of the storm-relative inflow angle in Z12, although their sample size is much smaller than ours. We then stratify the inflow angle into three groups by the shear magnitude: weak shear (≤5 m s^{-1}), moderate shear (5–10 m s^{-1}), and high shear (≥10 m s^{-1}) (Figure 3c). The inflow angle difference close to R_{max} (1–3 r^*) among these shear groups is relatively small, but the difference appears to be much larger in the outer core region (4–8 r^*), where the inflow angle in the weak- and moderate-shear groups is larger than that of the high-shear group.

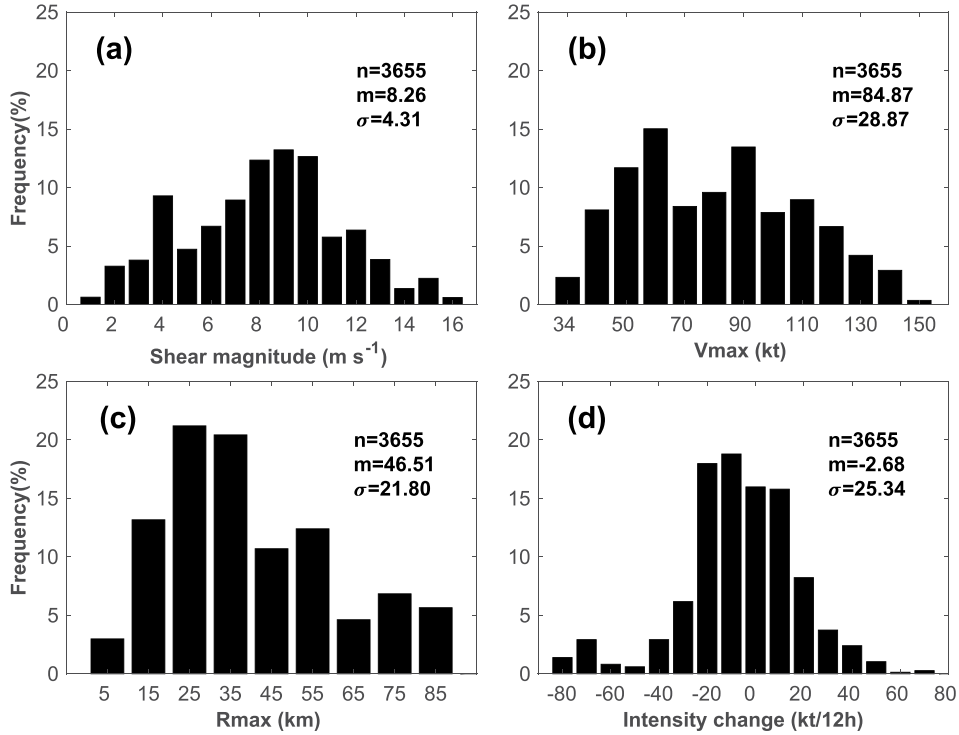

Figure 1. Frequency distribution of (a) shear magnitude, (b) storm intensity, (c) radius of the maximum wind speed (R_{max}), and (d) intensity change. The sample size (n), mean value (m), and standard deviation (σ) are also shown.

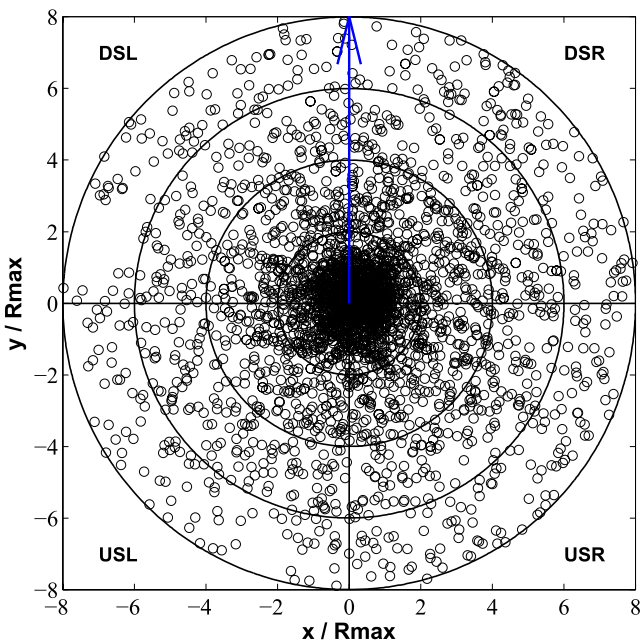

Figure 2. Plot of horizontal distribution of the dropsonde data. The shear direction is denoted by the blue arrow. DSL, DSR, USL, and USR represent downshear-left, downshear-right, upshear-left, and upshear-right quadrant, respectively. R_{max} is the radius of maximum surface wind speed.

The radial distribution of inflow angle in storms with different intensity change rates is compared in Figure 3d for intensifying ($\Delta V_{max}/\Delta t \geq 10kt/12h$) and steady-state ($5kt/12h > \Delta V_{max}/\Delta t \geq -5kt/12h$) groups. The mean inflow angle difference among the groups was relatively small close to the eyewall ($r^* < 3$). In the outer core region ($r^* > 3$), intensifying cases have a smaller magnitude of inflow angle than steady-state cases. The smaller inflow angle indicates longer residence time for air parcels to travel from the outer core region to the eyewall, which may allow for more accumulated surface enthalpy fluxes for intensification of the storm, assuming there is not a systematic difference in the 10-m winds and air-sea disequilibrium of enthalpy.

3.2. Shear-Relative Azimuthal Variation

Figure 4 shows the shear-relative azimuthal distribution of the inflow angle. The magnitude of the inflow angle on the downshear side is larger than that on the upshear side for all groups, with the maximum being downshear (Figure 4a). This result is consistent with convection being observed to be initiated on the downshear side more frequently than on the upshear side as shown in previous studies (e.g., Black et al., 2002; DeHart et al., 2014; Molinari et al., 2012; Reasor et al., 2013; Wadler et al., 2018; Zhang et al., 2013). Larger inflow angle downshear implies greater boundary-layer inflow and convergence, which supports convective initiation due to mass continuity. The azimuthal variation of inflow angle for the weak-shear group is minimal, while that in the moderate- and high-shear groups shows a larger degree of asymmetry (Figures 4b–4d). The amplitudes of wavenumber-1 asymmetry were evaluated by fitting the data with a cosine function in a

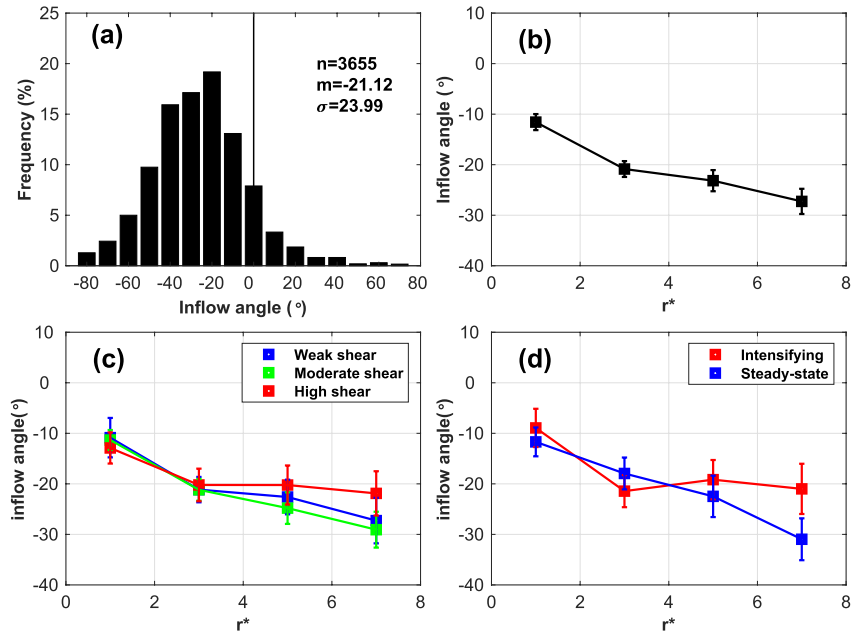

Figure 3. (a) Frequency distribution of surface inflow angle, n is sample size, m is mean value, σ is standard deviation, (b) plot of inflow angle as a function of radius normalized by the radius of maximum wind (r^*), (c) plots of inflow angle as a function of normalized radius for three shear magnitude groups: weak shear ($\leq$5 m s^{-1}; blue squares, sample size of 722), moderate shear (5 m s^{-1} < shear < 10 m s^{-1}; green squares, sample size of 1,678), and high shear ($\geq$10 m s^{-1}; red squares, sample size of 876), and (d) inflow angle as a function of normalized radius for intensifying (with a sample size of 654) and steady-state (with a sample size of 958) groups. Squares and error bars are bin averages and 95% confidence intervals, respectively.

similar manner as in Z12. We first calculate the difference between the mean value and maximum value of the fitted curve, and the difference between the mean value and minimum value of the fitted curve, respectively. Then taking the mean value of the two differences as the amplitude of the fitted curve, the amplitudes are 7.76°, 14.24°, 22.93° for weak-shear, moderate-shear and high-shear groups, respectively. Overall, the amplitude of the inflow angle asymmetry increases with the shear magnitude. We also test the statistical significance of the same azimuthal bin between different shear magnitudes through a student's t-test. As the numbers in Figures 4b–4d show, the differences are significant at the 95% or 90% confidence level for almost every azimuthal bin, indicating that the differences in azimuthal inflow angle among groups with different shear magnitudes are significant for almost all shear-relative quadrants. Furthermore, the differences between the 0° and 180° bins for weak, moderate, and high shear are significant at the 95% confidence interval. These results suggest a positive feedback between asymmetric convection and shear-induced overturning circulation that increases the inflow asymmetry, consistent with the schematic diagram given by Wong and Chan (2004, see their Figure 13).

To assess how the shear-relative azimuthal variation of inflow angle varies with radius, the data were divided into two additional groups based on radial locations that represent the eyewall region ($0.5 < r^* < 1.5$) and outer core region ($2.5 < r^* < 7.5$). Interestingly, the shear-relative inflow angle asymmetry in the eyewall region is smaller than that in the outer region for all three shear magnitude groups (Figure 5). The asymmetry amplitudes obtained by the cosine fitting of the data in the eyewall region are 2.13°, 6.86°, and 12.16° for the weak-, moderate-, and high-shear groups, respectively. On the other hand, the asymmetry amplitudes in the outer core region are 8.40°, 14.53°, and 21.59° for the three shear groups. For the same shear group, the amplitude is always larger in the outer core than eyewall, which means there is a stronger azimuthal asymmetry in inflow angle in the outer core. Previous numerical studies also showed that a sheared storm has more asymmetric low-level structure in the outer core than in the inner core region (Jones, 1995; Li & Wang, 2012), consistent with our observations.

The asymmetry amplitudes for the three shear groups in the outer core give a probable interpretation for the smaller axisymmetric inflow angle seen for high shear in the outer core shown in Figure 3c. As the asymmetry increases (Figures 5b, 5d and 5f), the inflow angle for high shear in the outer core can be positive on the upshear

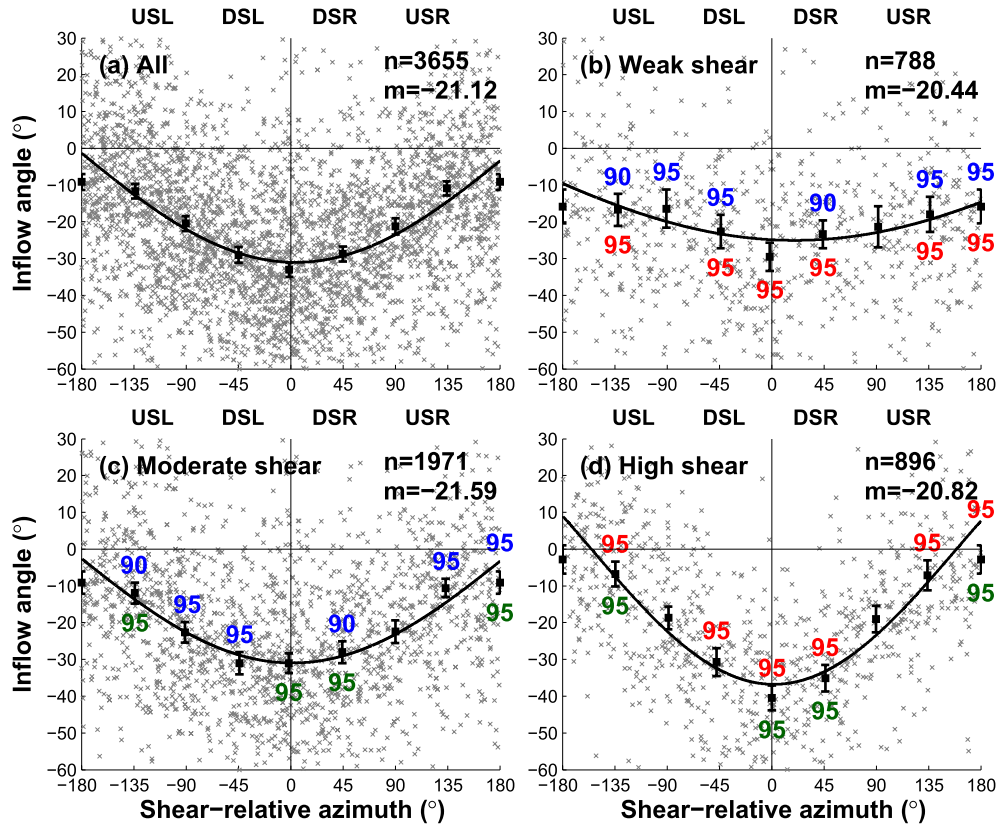

Figure 4. Azimuthal variation of inflow angle (a) for the full sample, (b) weak shear (shear ≤5 m s^{-1}), (c) moderate shear (5 m s^{-1} < shear <10 m s^{-1}) and (d) high shear (shear ≥ 10 m s^{-1}). The sample size (n), mean value (m) are also shown. Gray "x" symbols are individual dropsonde observations. The azimuthal angle is measured clockwise from the shear direction. Solid lines are cosine function fits. Black squares and error bars are bin averages and 95% confidence intervals respectively. The blue, red, and green numbers in (b–d) represent confidence interval percentages associated with the statistically significant differences for weak versus moderate shear, weak versus high shear, and moderate versus high shear groups, respectively.

side, offsetting the most negative values and resulting in the smaller mean inflow angle. As for the significance test, the differences between different shear groups are more significant in the outer core than in the eyewall. And the differences between the eyewall and outer core are more often at the bins of 0° and 180°. Additionally, the only comparison that is not significant at the 95% confidence interval between 0° and 180° bins is the difference in the weak shear group in the eyewall, which is consistent with its weak asymmetry.

This result from Figure 5 indicates that the extent of inflow angle asymmetry increases with the shear magnitude in both the eyewall and outer core regions. Previous numerical results on TC convective structure and distribution under different ranges of vertical wind shear showed similar differences in asymmetry magnitude among shear groups in the eyewall and outer regions (Li & Dai, 2020; Tao & Zhang, 2014). These results suggest that increasing shear drives an increase in the azimuthal inflow asymmetry and the asymmetry of the convective distribution.

3.3. Shear-Relative Distribution and TC Intensity Change in Moderate Shear

We next assess the shear-relative azimuthal variability of inflow angle with respect to TC intensity change rates with a focus on the moderate-shear group. We focus on this range of shear magnitude because it is in this range that there is the largest difficulty in accurately predicting intensity change (Bhatia & Nolan, 2013; Finocchio & Majumdar, 2017; Tao & Zhang, 2015). Furthermore, the sample size is the largest in the moderate shear group, compared to the weak or high shear groups.

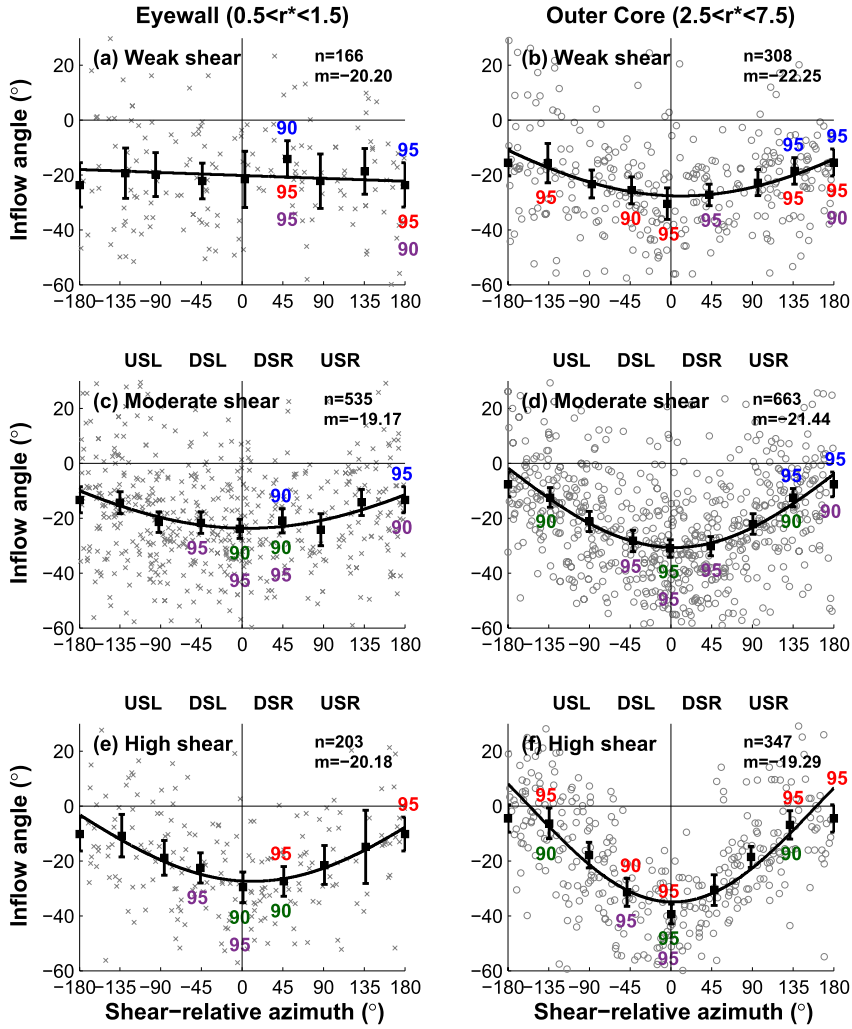

Figure 5. Azimuthal variation in inflow angle (left) near the eyewall ($0.5 < r^* < 1.5$; gray "x" symbols) and (right) outside the core ($2.5 < r^* < 7.5$; gray "o" symbols) for (a), (b) weak shear (shear ≤5 m s^{-1}), (c), (d) moderate shear (5 m s^{-1} < shear < 10 m s^{-1}), and (e), (f) high shear (shear ≥10 m s^{-1}) groups. The sample size (n), mean value (m) are also shown. Note that gray "x" and "o" symbols are observations from individual dropsondes. Solid black lines are cosine function fits. Black squares and error bars show bin averages and 95% confidence intervals respectively. The blue, red, and green numbers represent confidence interval percentages associated with the statistically significant differences for weak versus moderate shear, weak versus high shear, and moderate versus high shear groups, respectively. The purple numbers represent confidence interval percentages associated with the statistically significant differences between the eyewall and outer core regions.

Figure 6 shows the azimuthal variation in the shear-relative inflow angle for intensifying and steady-state groups in both the eyewall and outer core regions. Regardless of the intensity change range, the degree of asymmetry is larger in the outer region than in the eyewall. This eyewall versus outer-core difference is similar to that when the data were grouped by shear magnitude for all intensity change rates shown earlier. In both the eyewall and outer regions, the results show that the degree of inflow angle asymmetry in the intensifying group is smaller than that in the steady-state group. The asymmetry amplitudes of intensifying and steady-state groups are 4.17° and 8.11° in the eyewall region and are 8.89° and 18.61° in the outer core region, respectively. Moreover, we test the statistical significance between different quadrants in the outer core region. The differences between downshear-right and upshear-right, and that between downshear-left and upshear-left quadrants for the steady-state group in the outer core are statistically significant at the 95% confidence interval, while the difference between the downshear-right and upshear-right quadrants for the intensifying group in the outer core is not significant. This result suggests that the inflow angle in the steady-state group has a greater degree of azimuthal asymmetry than in the intensifying group, and that difference is maximized in the outer core.

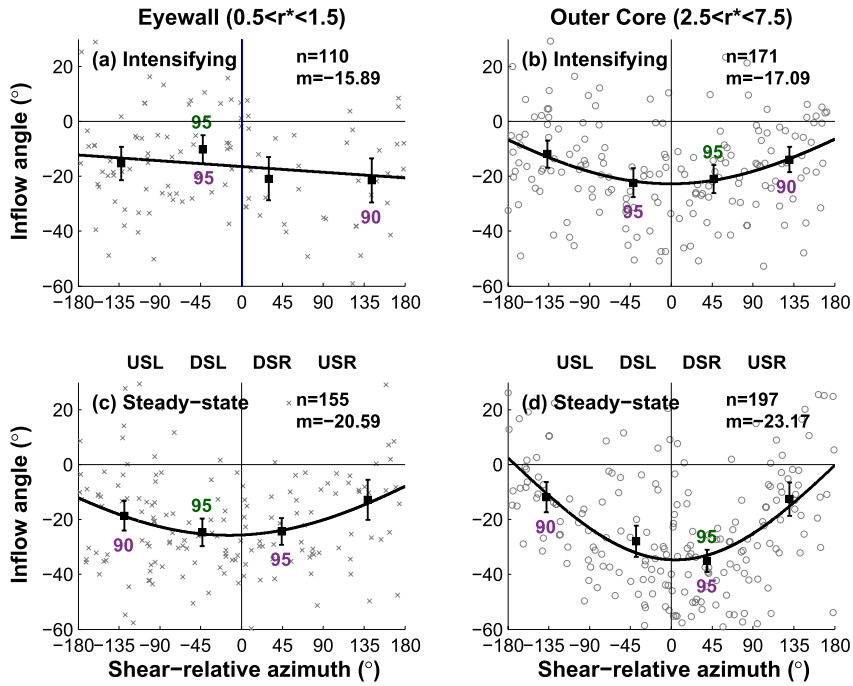

Figure 6. Azimuthal variation of inflow angle (left) in the eyewall ($0.5 < r^* < 1.5$; gray "x" symbols) and (right) the outer core region ($2.5 < r^* < 7.5$; gray "o" symbols) for (a), (b) intensifying, and (c), (d) steady-state storms under moderate shear (5 m s^{-1} < shear < 10 m s^{-1}). The sample size (n), mean value (m) are also shown. Note that gray "x" and "o" symbols are observations from individual dropsondes. Solid black lines are cosine function fits. Black squares and error bars show bin averages and 95% confidence intervals respectively. The green numbers represent confidence interval percentages associated with the statistically significant differences between intensifying and steady-state storms. The purple numbers represent confidence interval percentages associated with the statistically significant differences between the eyewall and outer core regions.

This result indicates that a more symmetric inflow distribution in the boundary layer favors TC intensification. Rogers et al. (2016) found that a more symmetric distribution of deep convection favors TC rapid intensification compared with an asymmetric distribution, supporting the idea that boundary layer convergence or inflow is more symmetrically distributed in intensifying storms, in agreement with our observations. Numerical studies (e.g., Tao & Zhang, 2019; Zhang & Rogers, 2019) also found that the most symmetric vortex structure was close to the onset of TC rapid intensification. Rios-Berrios and Torn (2017) showed that both the mid-tropospheric relative humidity and surface latent heat fluxes are more symmetric in intensifying storms than in steady-state storms, suggesting a potential linkage of the boundary layer inflow, surface flux and mid-level thermal structure in TCs and the important role of their azimuthal distributions in intensity change.

4. Conclusions

A composite analysis was conducted to investigate the distribution of the surface inflow angle in hurricanes with different intensity change rates under different environmental shear conditions using a total of 3,655 dropsondes from 44 storms. The results showed that the mean inflow angle for the full sample was −21.12°, which confirms that the axisymmetric radial flow from all samples is inflow. Furthermore, the magnitude of the axisymmetric inflow angle increases with the radial distance from the center, in agreement with the findings of Z12.

In terms of the radial variation of the azimuthally-averaged inflow angle, the magnitude of the inflow angle close to the eyewall region ($r^* < 2$) is comparable among the different shear magnitude and intensity change groups. The magnitude of the azimuthally-averaged inflow angle in the outer region ($r^* > 3$) decreases with increasing shear magnitude and is smaller in intensifying storms than in steady-state storms.

There is a shear-relative asymmetry in the inflow angle that varies with shear magnitude and intensity change, with the inflow angle magnitude, on average, larger on the downshear side. This asymmetry pattern appears in

both the eyewall and outer-core regions. The amplitude of the shear-relative inflow angle asymmetry increases with the shear magnitude in both regions. Regardless of intensity change rate, the degree of inflow angle asymmetry is larger in the outer core region than in the eyewall region.

The shear-relative distribution of the inflow angle was also examined in storms with different intensity change rates for the moderate shear group. In both the eyewall and outer core regions, the degree of inflow angle asymmetry in the intensifying group was smaller than that in the steady-state group. The largest inflow angle magnitude is located in the downshear to downshear-right side of the storm in the outer core within the steady-state group. The more symmetric boundary layer inflow could potentially lead to more symmetric convergence and forced convection immediately out of the boundary layer (Miyamoto & Takemi, 2015; Zhang & Rogers, 2019) and in turn affect deep convection distribution under similar instability conditions.

Notably, the focus in this paper has been on documenting the relationship between inflow angle and shear magnitude as well as that between inflow angle and TC intensity change. Future work will explore the combined effects of storm motion and environmental shear on the inflow angle distribution and its relationship to intensity change, mostly using a numerical approach given that a much larger observational data set than that used in this study is required. "Constructive" versus "destructive" interference of azimuthal asymmetries in the inflow angle driven by translation, phasing favorably or unfavorably with asymmetries driven by shear, and its relationship to TC intensity change will be investigated in this framework. Future work will also evaluate the impacts of different types of shear on the asymmetric distributions of inflow angle and convection. The relationships documented through this work can additionally be evaluated in numerical models and wind products used to drive storm surge models, providing a means of improving the structure of the surface wind field and associated surge prediction.

Data Availability Statement

The dropsonde data used in this study can be accessed from the Hurricane Research Division of National Oceanic and Atmospheric Administration's Atlantic Oceanographic and Meteorological Laboratory through the website: https://www.aoml.noaa.gov/hrd/data_sub/hurr.html. The SHIPS data used in this study can be accessed from https://rammb.cira.colostate.edu/research/tropical_cyclones/ships/developmental_data.asp website.

Acknowledgments
Jie Ming acknowledges support from the National Natural Science Foundation of China (Grant 42192555) and Fundamental Research Funds for the Central Universities (No. 020714380171). Jun Zhang acknowledges support from the U.S. Office of Naval Research Grant N00014-20-1-2071 and National Oceanic and Atmospheric Administration Grants NA21OAR4590370 and NA19OAR0220186. We are grateful to Frank Marks for his comments that lead to improvement of our paper.

References

Aijaz, S., Kepert, J. D., Ye, H., Huang, Z., & Hawksford, A. (2019). Bias correction of tropical cyclone parameters in the ECMWF ensemble prediction system in Australia. *Monthly Weather Review*, *147*(11), 4261–4285. https://doi.org/10.1175/MWR-D-18-0377.1

Barnes, G. M. (2008). Atypical thermodynamic profiles in hurricanes. *Monthly Weather Review*, *136*(2), 631–643. https://doi.org/10.1175/2007MWR2033.1

Bhatia, K. T., & Nolan, D. S. (2013). Relating the skill of tropical cyclone intensity forecasts to the synoptic environment. *Weather and Forecasting*, *28*(4), 961–980. https://doi.org/10.1175/WAF-D-12-00110.1

Black, M. L., Gamache, J. F., Marks, F. D., Jr., Samsury, C. E., & Willoughby, H. E. (2002). Eastern Pacific hurricanes Jimena of 1991 and Olivia of 1994: The effect of vertical shear on structure and intensity. *Monthly Weather Review*, *130*(9), 2291–2312. https://doi.org/10.1175/1520-0493(2002)130<2291:EPHJOA>2.0.CO;2

Bretschneider, C. L. (1972). A nondimensional stationary hurricane wave model. In *Paper Presented at the Offshore Technology Conference, Houston, Texas*. https://doi.org/10.4043/1517-MS

Bryan, G. H. (2012). Effects of surface exchange coefficients and turbulence length scales on the intensity and structure of numerically simulated hurricanes. *Monthly Weather Review*, *140*(4), 1125–1143. https://doi.org/10.1175/MWR-D-11-00231.1

Chavas, D. R., & Lin, N. (2016). A model for the complete radial structure of the tropical cyclone wind field. Part II: Wind field variability. *Journal of the Atmospheric Sciences*, *73*(8), 3093–3113. https://doi.org/10.1175/JAS-D-15-0185.1

Corbosiero, K. L., & Molinari, J. (2002). The effects of vertical wind shear on the distribution of convection in tropical cyclones. *Monthly Weather Review*, *130*(8), 2110–2123. https://doi.org/10.1175/1520-0493(2002)130<2110:TEOVWS>2.0.CO;2

DeHart, J. C., Houze, R. A., Jr., & Rogers, R. F. (2014). Quadrant distribution of tropical cyclone inner-core kinematics in relation to environmental shear. *Journal of the Atmospheric Sciences*, *71*(7), 2713–2732. https://doi.org/10.1175/JAS-D-13-0298.1

DeMaria, M., Mainelli, M., Shay, L. K., Knaff, J. A., & Kaplan, J. (2005). Further improvements to the statistical hurricane intensity prediction scheme (SHIPS). *Weather and Forecasting*, *20*(4), 531–543. https://doi.org/10.1175/waf862.1

Fan, S., Zhang, B., Mouche, A. A., Perrie, W., Zhang, J., & Zhang, G. (2020). Estimation of wind direction in tropical cyclones using C-band dual-polarization synthetic aperture radar. *IEEE Transactions on Geoscience and Remote Sensing*, *58*(2), 1450–1462. https://doi.org/10.1109/TGRS.2019.2946885

Fan, Y., Ginis, I., Hara, T., Wright, C. W., & Walsh, E. J. (2009). Numerical simulations and observations of surface wave fields under an extreme tropical cyclone. *Journal of Physical Oceanography*, *39*(9), 2097–2116. https://doi.org/10.1175/2009JPO4224.1

Finocchio, P. M., & Majumdar, S. J. (2017). The predictability of idealized tropical cyclones in environments with time-varying vertical wind shear. *Journal of Advances in Modeling Earth Systems*, *9*(8), 2836–2862. https://doi.org/10.1002/2017MS001168

Frank, W. M., & Ritchie, E. A. (2001). Effects of vertical wind shear on the intensity and structure of numerically simulated hurricanes. *Monthly Weather Review*, *129*(9), 2249–2269. https://doi.org/10.1175/1520-0493(2001)129<2249:EOVWSO>2.0.CO;2

Hock, T. F., & Franklin, J. L. (1999). The NCAR GPS dropwindsonde. *Bulletin of the American Meteorological Society*, *80*(3), 407–420. https://doi.org/10.1175/1520-0477(1999)080<0407:TNGD>2.0.CO;2

Holland, G. J. (1980). An analytic model of the wind and pressure profiles in hurricanes. *Monthly Weather Review*, *108*(8), 1212–1218. https://doi.org/10.1175/1520-0493(1980)108<1212:AAMOTW>2.0.CO;2

Houston, S. H., Shaffer, W. A., Powell, M. D., & Chen, J. (1999). Comparisons of HRD and SLOSH surface wind fields in hurricanes: Implications for storm surge modeling. *Weather and Forecasting*, *14*(5), 671–686. https://doi.org/10.1175/1520-0434(1999)014<0671:COHASS>2.0.CO;2

Jones, S. C. (1995). The evolution of vortices in vertical shear: Initially barotropic vortices. *Quarterly Journal of the Royal Meteorological Society*, *121*(524), 821–851. https://doi.org/10.1002/qj.49712152406

Kepert, J. D. (2010). Slab- and height-resolving models of the tropical cyclone boundary layer. Part I: Comparing the simulations. *Quarterly Journal of the Royal Meteorological Society*, *136*(652), 1686–1699. https://doi.org/10.1002/qj.667

Li, Q., & Dai, Y. (2020). Revisiting azimuthally asymmetric moist instability in the outer core of sheared tropical cyclones. *Monthly Weather Review*, *148*(3), 1297–1319. https://doi.org/10.1175/MWR-D-19-0004.1

Li, Q., & Wang, Y. (2012). Formation and quasi-periodic behavior of outer spiral rainbands in a numerically simulated tropical cyclone. *Journal of the Atmospheric Sciences*, *69*(3), 997–1020. https://doi.org/10.1175/2011JAS3690.1

Lin, N., & Chavas, D. (2012). On hurricane parametric wind and applications in storm surge modeling. *Journal of Geophysical Research*, *117*(D9). https://doi.org/10.1029/2011JD017126

Malkus, J. S., & Riehl, H. (1960). On the dynamics and energy transformations in steady-state hurricanes. *Tellus*, *12*(1), 1–20. https://doi.org/10.1111/j.2153-3490.1960.tb01279.x

Miyamoto, Y., & Takemi, T. (2015). A triggering mechanism for rapid intensification of tropical cyclones. *Journal of the Atmospheric Sciences*, *72*(7), 2666–2681. https://doi.org/10.1175/JAS-D-14-0193.1

Molinari, J., Romps, D. M., Vollaro, D., & Nguyen, L. (2012). CAPE in tropical cyclones. *Journal of the Atmospheric Sciences*, *69*(8), 2452–2463. https://doi.org/10.1175/JAS-D-11-0254.1

Molinari, J., & Vollaro, D. (2008). Extreme helicity and intense convective towers in hurricane bonnie. *Monthly Weather Review*, *136*(11), 4355–4372. https://doi.org/10.1175/2008MWR2423.1

Molinari, J., Vollaro, D., & Corbosiero, K. L. (2004). Tropical cyclone formation in a sheared environment: A case study. *Journal of the Atmospheric Sciences*, *61*(21), 2493–2509. https://doi.org/10.1175/jas3291.1

Nguyen, L. T., Rogers, R., Zawislak, J., & Zhang, J. A. (2019). Assessing the influence of convective downdrafts and surface enthalpy fluxes on tropical cyclone intensity change in moderate vertical wind shear. *Monthly Weather Review*, *147*(10), 3519–3534. https://doi.org/10.1175/MWR-D-18-0461.1

Onderlinde, M. J., & Nolan, D. S. (2017). The tropical cyclone response to changing wind shear using the method of time-varying point-downscaling. *Journal of Advances in Modeling Earth Systems*, 9(2), 908–931. https://doi.org/10.1002/2016MS000796

Peng, M., Xie, L., & Pietrafesa, L. J. (2006). Tropical cyclone induced asymmetry of sea level surge and fall and its presentation in a storm surge model with parametric wind fields. *Ocean Modelling*, *14*(1), 81–101. https://doi.org/10.1016/j.ocemod.2006.03.004

Powell, M. D. (1982). The transition of the Hurricane Frederic boundary-layer wind field from the open Gulf of Mexico to landfall. *Monthly Weather Review*, *110*(12), 1912–1932. https://doi.org/10.1175/1520-0493(1982)110<1912:ttothf>2.0.co;2

Powell, M. D., Uhlhorn, E. W., & Kepert, J. D. (2009). Estimating maximum surface winds from hurricane reconnaissance measurements. *Weather and Forecasting*, *24*(3), 868–883. https://doi.org/10.1175/2008WAF2007087.1

Queensland Government. (2001). *Queensland climate change and community vulnerability to tropical cyclones: Ocean hazards assessment—stage 1, J0004–PR0001C* (p. 383). Department of Natural Resources and Mines.

Reasor, P. D., Eastin, M. D., & Gamache, J. F. (2009). Rapidly intensifying hurricane Guillermo (1997). Part I: Low-wavenumber structure and evolution. *Monthly Weather Review*, *137*(2), 603–631. https://doi.org/10.1175/2008MWR2487.1

Reasor, P. D., Rogers, R., & Lorsolo, S. (2013). Environmental flow impacts on tropical cyclone structure diagnosed from airborne Doppler radar composites. *Monthly Weather Review*, *141*(9), 2949–2969. https://doi.org/10.1175/MWR-D-12-00334.1

Rios-Berrios, R., Davis, C. A., & Torn, R. D. (2018). A hypothesis for the intensification of tropical cyclones under moderate vertical wind shear. *Journal of the Atmospheric Sciences*, *75*(12), 4149–4173. https://doi.org/10.1175/JAS-D-18-0070.1

Rios-Berrios, R., & Torn, R. D. (2017). Climatological analysis of tropical cyclone intensity changes under moderate vertical wind shear. *Monthly Weather Review*, *145*(5), 1717–1738. https://doi.org/10.1175/MWR-D-16-0350.1

Rogers, R. F., Reasor, P. D., Zawislak, J. A., & Nguyen, L. T. (2020). Precipitation processes and vortex alignment during the intensification of a weak tropical cyclone in moderate vertical shear. *Monthly Weather Review*, *148*(5), 1899–1929. https://doi.org/10.1175/MWR-D-19-0315.1

Rogers, R. F., Zhang, J. A., Zawislak, J., Jiang, H., Alvey, G. R., III, Zipser, E. J., & Stevenson, S. N. (2016). Observations of the structure and evolution of Hurricane Edouard (2014) during intensity change. Part II: Kinematic structure and the distribution of deep convection. *Monthly Weather Review*, *144*(9), 3355–3376. https://doi.org/10.1175/MWR-D-16-0017.1

Ryglicki, D. R., Cossuth, J. H., Hodyss, D., & Doyle, J. D. (2018). The unexpected rapid intensification of tropical cyclones in moderate vertical wind shear. Part I: Overview and observations. *Monthly Weather Review*, *146*(11), 3773–3800. https://doi.org/10.1175/MWR-D-18-0020.1

Ryglicki, D. R., Doyle, J. D., Hodyss, D., Cossuth, J. H., Jin, Y., Viner, K. C., & Schmidt, J. M. (2019). The unexpected rapid intensification of tropical cyclones in moderate vertical wind shear. Part III: Outflow–environment interaction. *Monthly Weather Review*, *147*(8), 2919–2940. https://doi.org/10.1175/MWR-D-18-0370.1

Tao, D., & Zhang, F. (2014). Effect of environmental shear, sea-surface temperature, and ambient moisture on the formation and predictability of tropical cyclones: An ensemble-mean perspective. *Journal of Advances in Modeling Earth Systems*, *6*(2), 384–404. https://doi.org/10.1002/2014MS000314

Tao, D., & Zhang, F. (2015). Effects of vertical wind shear on the predictability of tropical cyclones: Practical versus intrinsic limit. *Journal of Advances in Modeling Earth Systems*, *7*(4), 1534–1553. https://doi.org/10.1002/2015MS000474

Tao, D., & Zhang, F. (2019). Evolution of dynamic and thermodynamic structures before and during rapid intensification of tropical cyclones: Sensitivity to vertical wind shear. *Monthly Weather Review*, *147*(4), 1171–1191. https://doi.org/10.1175/MWR-D-18-0173.1

Wadler, J. B., Rogers, R. F., & Reasor, P. D. (2018). The relationship between spatial variations in the structure of convective bursts and tropical cyclone intensification as determined by airborne Doppler radar. *Monthly Weather Review*, *146*(3), 761–780. https://doi.org/10.1175/MWR-D-17-0213.1

Wadler, J. B., Zhang, J. A., Rogers, R. F., Jaimes, B., & Shay, L. K. (2021). The rapid intensification of Hurricane Michael (2018): Storm structure and the relationship to environmental and air–sea interactions. *Monthly Weather Review*, *149*(1), 245–267. https://doi.org/10.1175/MWR-D-20-0145.1

Wang, W., Sippel, J. A., Abarca, S., Zhu, L., Liu, B., Zhang, Z., et al. (2018). Improving NCEP HWRF simulations of surface wind and inflow angle in the eyewall area. *Weather and Forecasting*, *33*(3), 887–898. https://doi.org/10.1175/WAF-D-17-0115.1

Willoughby, H. E. (1990). Gradient balance in tropical cyclones. *Journal of the Atmospheric Sciences*, *47*(2), 265–274. https://doi.org/10.1175/1520-0469(1990)047<0265:GBITC>2.0.CO;2

Wong, M. L. M., & Chan, J. C. L. (2004). Tropical cyclone intensity in vertical wind shear. *Journal of the Atmospheric Sciences*, *61*(15), 1859–1876. https://doi.org/10.1175/1520-0469(2004)061<1859:TCIIVW>2.0.CO;2

Zhang, H., Chen, D., Zhou, L., Liu, X., Ding, T., & Zhou, B. (2016). Upper ocean response to typhoon Kalmaegi (2014). *Journal of Geophysical Research: Oceans*, *121*(8), 6520–6535. https://doi.org/10.1002/2016JC012064

Zhang, J. A., Dunion, J. P., & Nolan, D. S. (2020). In situ observations of the diurnal variation in the boundary layer of mature hurricanes. *Geophysical Research Letters*, *47*(3), e2019GL086206. https://doi.org/10.1029/2019GL086206

Zhang, J. A., Nolan, D. S., Rogers, R. F., & Tallapragada, V. (2015). Evaluating the impact of improvements in the boundary layer parameterization on hurricane intensity and structure forecasts in HWRF. *Monthly Weather Review*, *143*(8), 3136–3155. https://doi.org/10.1175/MWR-D-14-00339.1

Zhang, J. A., & Rogers, R. F. (2019). Effects of parameterized boundary layer structure on hurricane rapid intensification in shear. *Monthly Weather Review*, *147*(3), 853–871. https://doi.org/10.1175/MWR-D-18-0010.1

Zhang, J. A., Rogers, R. F., Reasor, P. D., Uhlhorn, E. W., & Marks, F. D., Jr. (2013). Asymmetric hurricane boundary layer structure from dropsonde composites in relation to the environmental vertical wind shear. *Monthly Weather Review*, *141*(11), 3968–3984. https://doi.org/10.1175/MWR-D-12-00335.1

Zhang, J. A., Rogers, R. F., & Tallapragada, V. (2017). Impact of parameterized boundary layer structure on tropical cyclone rapid intensification forecasts in HWRF. *Monthly Weather Review*, *145*(4), 1413–1426. https://doi.org/10.1175/MWR-D-16-0129.1

Zhang, J. A., & Uhlhorn, E. W. (2012). Hurricane sea surface inflow angle and an observation-based parametric model. *Monthly Weather Review*, *140*(11), 3587–3605. https://doi.org/10.1175/MWR-D-11-00339.1

Zhao, W., & Hong, X. (2011). Impacts of tropical cyclone inflow angle on ocean surface waves. *Chinese Journal of Oceanology and Limnology*, *29*(2), 460–469. https://doi.org/10.1007/s00343-011-0194-4